Accuracy of 'J'orographic Maps Derived from ERS-1Interferometric Radar

HOWARD A. ZEBKER, CHARLES L. WERNER, PAUL ROSEN, AND SCOTT HENSLEY
Jet Propulsion Laboratory
California Institute of Technology
4800 Oak Grove Drive
Pasadena, CA 91109

March 23, 1993

To be submitted to:
IEEE Transactions 011 Geoscience and Remote Sensing

Please address correspondence to:
Howard A. Zebker
MS 300-227
Jet Propulsion Laboratory
4800 Oak Grove Drive
Pasadena, CA 91109
Tel.(818) 354-8780, FAX(818)354-9476

A radar interferometric technique for topographic mapping of surfaces promises a high resolution approach to generation of digital elevation models. We present here analyses of data collected by the synthetic aperture radar instrument on board the ERS-1 satellite on successive orbits, Using a single satellite in a nearly repeating orbit is attractive for reducing cost and spaceborne hardware complexity; also it permits inference of changes in the surface from the correlation properties of the radar echoes. The data have been reduced to correlation maps and digital elevation models. The correlation maps show that temporal correlation decreases significantly with time, but not necessarily at a constant, well-defined rate, likely depending on environmental factors. When correlation) among passes remains high, however, it is possible to form digital elevation models. Analysis of noise expected in ERS-1 interferometric data collected over Alaska and the southwestern U.S. indicates that maps with relative errors less than 5 m rms are possible in some regions. However, orbit uncertainties imply that tic points arc required in order to reduce absolute height errors to a similar magnitude. We find that about 6 tiepoints per 4(I by 40 km scene with 5 m or better rms height accuracy arc needed to keep systematic map height errors below 5 m rms. The performance of the ERS-1 radar system for topographic applications, though useful for a variety of regional and local discipline studies, may be improved with respect to temporal decorrelation errors and absolute height acuity by modifying the orbit repeat period and incorporating precise orbit determination techniques. The resulting implementation will meet many, but not all, objectives of a global mapping mission.

Introduction

Radar interferometry is now gaining increasing credibility as a technique for rapid, accurate topographic data collection. As digital elevation models produced in this manner arc becoming avail able to the general science and operational communities, and as a number of interferometric radar systems arc in the planning and implementation stages, it is important to understand the accuracy and limitations of the technique. In this paper we examine the credibility and usefulness of interferometric radar topographic data generated by one particular implementation, the ERS-1 radar system, which generates interferometric information by combining data from two successive passes of tile satellite over a given surface region. here we will briefly review theoretical concepts, estimate performance from the ERS-1 radar system parameters, present DEMs produced by the system, demonst rate that to obtain high absolute accuracies known image tie points are needed, and finally discuss the possibili ty of using the ERS-1 system to generate a global, consistent topographic map.

A radar interferometer is formed by relating the signals from two spatially separated radar antennas; the separation of the two antennas is called the baseline. The two antennas may be mounted on a single platform, the usual implementation for aircraft systems [1,2], or a synthetic

interferometer may be realized by utilizing a single antenna on a satellite in a nearly-exact repeating orbit- in this case the interferometer baseline is formed by relating radar signals on repeat passes over tile same site. Even though the antennas do not illuminate the same area at the same time, if tile ground is completely undisturbed between viewings tile two sets of signals will be highly correlated and a spatial baseline may be synthesized. Topographic maps using this technique have been demonstrated by Goldstein *et al.* [3], Gabriel *et al.* [4], Gabriel and Goldstein [5], and Zebker and Villasenor [6].

The performance of a radar interferometer system depends on the radar instrument parameters, the orbit parameters, and the errors induced by the data processing and post processing operations. For the repeat- pass implementation in particular, temporal decorrelation constitutes an important and in many cases the limiting error source in the operation of a topographic mapping radar. Zebker and Villasenor [6] investigated temporal decorrelation phenomena for the SEASAT 24 cm-λ (L-band) radar and were able to determine rates of decorrelation for several types of surfaces. We analyze here ERS-1 6 cm-λ (C-band) data and find that the decorrelation rates are often so much higher than in the SEASAT case that it is difficult to measure the rate given the three-day sampling of the surface provided by the satellite orbit. L\'lie]\ the correlation drops significantly, the utility of the topographic maps derived from the radar measurements is limited. Prati *et al.* [7] have reported similar decorrelation effects in ER - 1 interferometric data over Europe.

Several problems are observed specific to the ERS-1 / Alaska SAR Facility (ASF) implementation. The coverage area of this system is limited by the need to downlink real-ti]nc data from the satellite to the Fairbanks, Alaska, receiving station, thus only data acquired over a 3000-km radius circle centered on the receiving antenna are available. As we will discuss below, high correlation may be achieved only when little weathering or other environmental change occurs- this is an important consideration in arctic regions. In addition, the small ERS-1 incidence angle of about 23° is far from optimum, as significant layover regions are observed which lead to gaps in the map that must be inter polated over. Finally, during the commissioning phase of the mission the ERS-1 orbit was adjusted many times so that large, unusable interferometer baselines often were the result. Despite these limitations, in certain cases topographic mapping is not only feasible but perhaps the only means to obtain high quality digital elevation data of selected sites.

Theoretical Summary: Height Equations and Error Sources

The theory of topographic mapping using radar interferometry has already been presented in some detail [1,2,6,8,9], so here we only summarize the main results and establish notation. For repeat pass imaging geometries, on each pass tile radar acts as both a transmitter and receiver, therefore the total path difference for each radar observation toa given point on the surfacers twice what would be expected if a single spacecraft or aircraft with two physical antennas is used. Thus, some Of the equations listed here differ from those in the references by a factor of two.

Given two antennas A1 and A2 as shown in figure 1 , surface topography as given by $z(y)$, the

spacecraft altitude h above ii tangent plane at the point of interest, the baseline distance B, the range to a point on the ground r, the look angle 0, and the angle of the baseline with respect to horizontal α, two radar signals transmitted from each antenna and received at the point of transmission will, when properly resampled and cross-multiplied, form an interferogram where the phase at each point is proportional to the difference in path lengths, 2δ, with the constant of proportionality $\frac{2\pi}{\lambda}$. A little algebra and geometry yield the following equations for height as a function of these parameters:

$$\delta = \frac{\lambda\phi}{4\pi} \tag{1}$$

$$\sin(\theta - \alpha) = \frac{(r + \delta)^2 - r^2 - B^2}{2rB} \tag{2}$$

$$z(r, \theta) = h - r\cos\theta \tag{3}$$

where ϕ is the measured phase, and λ is the wavelength.

Differentiation of (1-3) with respect to ϕ yields the error in llci.gilt estimate as a function of the error in phase estimate to first order:

$$\sigma_z = \frac{\lambda r}{4\pi B}[\sin\alpha - \cos\alpha\tan(\alpha - \theta)]\,\sigma_\phi \tag{4}$$

where σ_z and σ_ϕ are the standard deviations of height and phase, respectively.

The second significant error source results from errors in knowledge of the synthetic interferometer baseline alignment, that is it is impossible to distinguish a baseline angle knowl edge error from a slope on tile surface topography, and therefore extremely precise knowledge of the baseline geometry is required if absolute height estimation is needed. Differentiation with respect to α yields

$$\sigma_z = r\sin\theta\sigma_\alpha \tag{5}$$

Since the principal effect from an attitude error is to introduce a tilt across the radar swath, accurate height measurements may still be achieved when a large uncertainty in α exists - this entails correcting the image heights with tie points to determine the absolute height values. This approach will be described in greater detail below.

Equation (5) can be rewritten explicitly in terms of the uncertainties in the horizontal and vertical components of the baseline σ_{B_y} and σ_{B_z} as:

$$\sigma_z = \frac{r}{B}\sin\theta\sin\alpha\,\sigma_{B_y} \tag{6a}$$

$$\sigma_z = \frac{r}{B}\sin\theta\cos\alpha\,\sigma_{B_z} \tag{6b}$$

This form of the uncertainty equations is useful when evaluating errors from traditional orbit position information.

It is important to realize that the above two types of errors are significantl y different in nature: the phase errors increase the statistical variation of each point in the DEM, while the attitude errors are systematic in that a large ground region will exhibit a common error. As stated previously, there is the opportunity to correct attitude errors using knowledge of the height of a few points in a given image scene.

Successful implementation of an interferometric topographic mapping instrument requires that both the uncertainty in the baseline components and the phase noise be minimized. Analysis of the former is straight-forward and results from characterizing the platform position for each orbit and applying compensation algorithms in the radar processor- the residual uncompensated baseline error determines the height error from (5) or (6). For conventional orbit determination precision, this error term is usually unacceptably large, however, as discussed previously, these errors can be reduced further by inference of the residual baseline components from known points in the scene (see more in tie point discussion] below).

The phase noise term results from various factors including thermal noise, sampling and processing artifacts, and correlation of the individual radar echoes before they are combined to form the interferogram. Each of these may be characterized either by an equivalent signal-to-noise ratio SNR or correlation ρ, which are related by [6]

$$\rho = \frac{1}{1 + \mathrm{SNR}^{-1}} \tag{7}$$

One common technique for reducing statistical noise in a signal is averaging, and for interferograms the optimal estimator in a maximum likelihood sense is to average spatially the complex signal values, as was shown by Rodriguez [10]. In radar jargon this is equivalent to 'taking looks' in order to reduce statistical variation. We plot in figure 2 phase noise σ_ϕ as a function of looks and correlation of the signals as determined by numerical simulation (figure 2 is an extension of work reported by Li and Goldstein [9]), As indicated in the figure, phase noise is reduced by maximizing both the number of looks and the correlation.

Processing artifacts such as sidelobes, quantization noise, interpolation noise, and defocussing can contribute to random and systematic phase errors in processed radar scenes and resulting interferograms. These random errors can be viewed as an effective loss in the SNR to be used in equation (7) when computing the thermal noise correlation coefficient. Defocussing will affect the absolute phase of an image or image pair. This kind of error is minimized in systems steered toa zero Doppler geometry as is the case with ERS-1, however inevitably some error will exist.

Decorrelation noise arises from several sources distinct from the already mentioned thermal effects and processing artifacts. Most important for radar interferometry in general and for repeat

pass implementations in particular are what we refer to as baseline and temporal decorrelation. (Rotation of the viewing angle is also important w'lien interferometric techniques are applied to satellites in crossing orbits [5], but these systems would never be practical for global mappi ng applications, and we will ignore this term here.) Baseline decorrelation results from viewing the surface at two slightly different look angles and increases with increasing differential angle (or baseline) [9]. The correlation between echoes varies approximately linearly, decreasing from unity at zero baseline to zero at a critical baseline

$$B_c \simeq \frac{\lambda r}{2 R_y \operatorname{Cos} \theta} \tag{8}$$

where R_y is the ground range resolution and θ is the local incidence angle. The critical baseline in (8) is measured perpendicular to the look direction; the component parallel to the look direction dots not affect the baseline decorrelation [6,8]. For optimal system performance, the baseline must be large enough to give sufficient phase sensitivity to height (eqs. 1-3), yet small enough as not to introduce too much decorrelation noise, therefore this defines a tradeoff in interferometer design. We note that this analysis is valid only for level surfaces. If there is significant topography, variations in the local incidence angle can reduce the largest baseline useful for topographic mapping.

The other important source of decorrelation for repeat pass mapping is temporal decorrelation. If we model a surface as consisting of a random collection of scatterers in each resolution element, and if the scatterers are undisturbed bet ween radar observ ations, then the scattering event is random but deterministic and the exact same signal will be received at the second observation as on the first observation, save for the above-mentioned thermal and spatial baseline effects. Zebker and Villa senor [6] show that correlation may be expressed as a function of the r-ins motion of the scat terers approximately by

$$\rho \simeq \exp\{-\frac{1}{2}(\frac{4\pi}{\lambda})^2(\hat{\sigma}_y^2 \sin^2\theta + \sigma_z^2 \cos^2\theta)\} \tag{9}$$

where σ_y and σ_z are the rms motions in the across track and vertical directions, respectively. They report this phenomenon as observed in SEASAT echoes obtained over Death Valley, CA, and Oregon forested regions over a 20 day period in Sc~)tc'lllLcr/October]978, and note for most types of terrain gradually decreasing correlation with time on the scale of days. Assessment of the utility of the ERS-1 radar data for topographic mapping thus requires an equivalent measurement for the shorter wavelength C-band data which by equation (9) is more sensitive to small surface change by a factor of four than the SE ASAT L-band signals.

Theoretical ERS-1 Interferometer Performance

In this section we estimate tile topographic mapping performance of the ERS-1 radar system in a repeat-pass con figuration. Some system parameters of the ERS-1 radar are given in Table 1.

Table 1. Nominal ERS-1 radar system parameters

Parameter	ERS-1 value
Wavelength, m	0.0566
Peak power, watts	4800
Pulse rate, Hz	1679 nominal
Pulse length, μ sec	37.1
Antenna length, m	10.0
Antenna width, m	1.0
Antenna gain, dB	43.2
Range bandwidth, MHz	15.55
Receiver noise temperature, K	3700
Integrated Sidelobe ratio, dB	-14
Quantization Noise (5 bit), dB	-30
Slant range resolution, m	10.2
Ground range resolution, m	25
Azimuth resolution, m	G
Orbit altitude, km	790
Incidence angle, deg	24
Orbit repeat interval, days	3, 35, 165

The radar system exhibits a typical signal to noise ratio of 11.7 dB as derived using the design control table shown in Table 2. This SNR corresponds (eq. 7) to a correlation of 0.94.

Table 2. ERS-1 radar design control table

Parameter	ERS-1value ill dB/dBW
Peak power	36.8
Antenna directional gain	45.9
Antenna efficiency	-3
$\frac{1}{4\pi}$	-11
$\frac{1}{R^2}$	-118.6
Illuminated area	78.4
σ^0	-14
$\frac{1}{4\pi}$	-11
$\frac{1}{R^2}$	-118.6
Antenna area	10
Antenna efficiency	-3
System losses	-3
Oversampling gain	1.8
Total	-109.3
Thermal noise (kTB)	-121.0
Signal to noise ratio	11.7

From (8), the critical baseline for ERS-1 is 1115 m. Observed ERS-1 orbits have repeat pass baselines of random orientation and highly variable length. For a typical observed orbit spacing perpendicular to the look direction of $B_\perp$ = 165 m, the baseline component of correlation is 0.85. Thus, the total correlation from baseline effects and signal to noise ratio under the above assumptions is 0.81. In order to *reduce* phase errors, we will assume that the interferogram is averaged, resulting in about 10 effective looks given by

$$N = \frac{A_p}{R_x R_y} \tag{lo}$$

where A_p is the ground area of the multilook pixel and R_x and R_y are the ground resolutions in azimuth and range. From figure 2 the phase error will be 11 degrees, which from (4) results in a statistical height error of 1.8 m rms.

This height error estimate corresponds to the case where 1) no errors are added by the radar data processing operations, and 2) no temporal decorrelation occurs. In this sense it represents a lower bound to statistical errors.

We next estimate the height errors induced by uncertainty in the baseline components, which in this case is dominated by uncertainties in orbit determination. Currently the best operational orbit

estimates for ER - 1 are about 30 cm [1 1]. For a horizontal baseline length of 180 m corresponding to $B_\perp$ = 165 m, (6) gives an absolute height error of order 1 km; clearly orbit determination alone cannot suffice for generation of topographic maps. It is important to realize again that this is a systematic error, that is it affects every point in the image with approximately the same error, and that in a relative sense the map may still be quite accurate, as indicated by the 1.8 m calculation above. Thus, a practical topographic mapping system using El{ S-l requires the use of tie points in the image or some other technique 10 produce useful topographic maps.

Observed El{ S-l Interferometer Performance

We have produced several topographic maps from ERS-1 observations and have used interferograms directly to estimate temporal decorrelation over multiples of the three day orbit repeat interval. We present in this section correlation observations over hit. Katmai, Toolik Lake, and Manley Hot Springs sites in mainland Alaska and of Shishaldin volcano in the Aleutian Islands. We then show digital elevation models of the Toolik and Manley sites and discuss the observed accuracy. Although we have examined over 10 pairs of images of the volcanic sites, none provided sufficient correlation over the entire scene to permit generation of a useful map. In order to show that given the right environmental conditions, however, correlation may be sustained over long time periods, we also show a DEM of the Pisgah lava flow area in California. These data were acquired from the Canadian receiving station at Prince Albert, Saskatchewan, when tile satellite was operating in the 35-day repeat cycle, showing that for scenes m'here no disturbances occur interferometric techniques are possible with very long temporal baselines.

Data]'recessing **Procedure.** The data we use here, with the exception of the data over tile southwestern U. S., are products of the Alaska SAR Facility, built by JPL and operated by tile University of Alaska at Fairbanks, Institute for Geophysical research, where the facility is located. The southwest 11 .S. data were recorded by tile Canadian Prince Albert receiving station. We requested standard complex products for each scene, and each was identified by a location in latitude and longitude and by date. As the three day orbit repeat corresponds to 43 orbits, orbit pairs with revolution numbers differing by 43 were requested. The complex images represent ground areas approximately 40 by 50 km, at a slant range pixel spacing of 7,9 m and an azimuth pixel spacing of about 3.9 in. The data are in complex format, with 16 bit representations for each of tile real and imaginary parts. One complex scene, two of which are needed to form each interferogram, has 2048 range elements and 12S00 azimuth lines for a total size of about 106 Mb.

The Canadian data are supplied in raw signal sample form and we processed these at JPL.

The next step in the data processing procedure is to determine the spatial offset of the two images at several locations. As slightly different look angles arc involved, the range and azimuth ofl'sets vary with range across the image. If the orbits are nearly parallel, as is tile case for all data analyzed here, we can assume that the range and azimuth spacing do not vary with azimuth. We calculate the offsets by cross multiplying a 32 by 32 pixel portion of one image by the complex

conjugate of a similar section in the other image and calculating the Fourier transform of the result. Since when the alignment is optimum the visibility of the interference fringes is high, in that instance the Fourier transform will exhibit a strong peak. We search a small range of integer pixel offsets until the maximum transform peak and several neighboring values are found. These are then interpolated quadratically to estimate the actual offset at that location. The entire process is repeated for different ranges, and the range-dependent offset functions are found by fitting a polynomial by least squares to the measured range and azimuth offsets.

Once the offsets are determined, one image is interpolated using a local quadratic polynomial to match the second image on a point for point basis. The two images are then cross multiplied, and typically 2 pixels in range and 10 in azimuth are averaged. Since the pixels are not entirely uncorrelated, the resulting interferogram exhibits statistical properties of roughly 10 look images.

Correlation measurements. The correlation coefficient at each of the multilook pixels is calculated according to

$$\rho = \frac{|E(c_1 c_2^*)|}{(E(c_1 c_1^*)E(c_2 c_2^*))^{\frac{1}{2}}} \tag{11}$$

where c_1 and c_2 are the corresponding complex values from the two images after interpolation. in this section we will display several correlation maps for regions in Alaska observed by ERS-1, where each pixel will be color coded such that the brightness of each point is related to the radar cross section and tile color is the correlation coefficient defined by (11), where the averaging interval is defined by each 2 by 10 pixel input field. For the purposes of this paper we are interested in indicating where correlation will be high enough to permit reasonable phase estimation. Accurately interpreting the observed correlation values in terms of geophysical factors of the ground is an interesting topic left for future work.

A summary of data sites investigated here, ERS-1 passes, and other ancillary information are given in Table 3.

Table 3. Sites and Data Acquisition Parameters

Site name	Lat.	Long.	Orbit pair	B, m [a]	$B_\perp$, m [b]	ρ_B [c]	ρ_T [d]
Toolik Lake	68.7 N	150.9 W	943, 1029	106.2	40.4	0.96	0.90
			1029, 1072	233.5	201,2	0.80	0.75
Manley not Springs	64.9 ?!	149.3 W	892, 935	177.8	155.9	0.84	0.79
hit. Katmai	58.3 N	155.0 W	943, 1029	144.2	44.5	0.95	0.89
			1459, 1502	99.3	62.0	0.94	0.88
Shishaldin Volcano	54.7 N	164.1 W	2670, 2713	48.7	44.3	0.95	0.89
Pisgah Lava Flow	34.5 N	116.3 W	5873, 6284	112.8	89.5	0.90	0.85

[a] Baseline

[b] Baseline component perpendicular to look direction; critical baseline $B_c = 1115$ m

[c] Baseline correlation

[d] Baseline + thermal correlation assuming SNR = 11.7 dB

Sample maps of the correlation coefficient for the Toolik site area are shown in figure 3. The color scale is such that zero correlation is represented by bluish purple, while unity correlation is given by yellowish green. The observed correlation coefficient depicted here is the product of all of the various factors affecting signal correlation, including thermal noise, spatial baseline noise, and temporal change noise. Since we can predict the former two with knowledge of the radar system parameters, dividing the observed correlation by the predicted value provides an estimate of the temporal decorrelation on a point by point basis. Two images are shown, one corresponding to a 6 day repeat interval and one to a 3 day interval. Note that the 6 day image is significantly more correlated than the 3 day image. Since signal to noise ratios are similar and baseline decorrelation for both cases is small (see Table 3), the temporal correlation is higher over the longer rather than the snorter time interval. Thus, environmental factors which occur sporadically rather than continuously over time are dominating the observed correlation.

The majority of the six day image possesses an average correlation of 0.50 or more, implying that for 10 look data phase errors are less t han 30°, which corresponds to height errors of 17.3 m (eq. 4), an unreasonably high limit for usable topographic maps. The three day image has large areas in which the correlation drops below half, however because tile projected baseline is five times longer than that of the 6 day data, the height errors are appreciably smaller. Most of this image has a correlation of 0.25 or above, implying height errors of 7,5111 or better, thus approaching a suitable error for topographic mapping.

Figure 4 depicts the correlation map measured over the Manley Hot Springs site, and it resembles in correlation properties the Toolik data, implying that topographic models derived from the data will be of useful quality. This contrasts with Figure 5, correlation images of the hit. Katmai area, in which large sect ions of the image are uncorrelated. While certain subsections exhibit very high

correlation values of about 0.85, only these small pieces may be expected to yield accurate phase estimates and hence useful digital elevation models. Examination of figure 5a shows some evidence of an elevation effect. particularly on Mt. Griggs, the large mountain near the image center. The average of the correlation coefficients exceeds 0.5 on the lower slopes of the mountain, but above a constant altitude it drops to nearly uncorrelated. This could indicate an elevation-dependent weather factor. The distribution of correlation values in figure 5b is less obviously related to altitude but appears 10 be highest in the valley floo Is.

Finally, in figure 6 wc show the correlation map Of Shishaldin volcano in the Aleutian Islands. The water is of course completely uncorrelated, as is the land area over much of the image. Only a few outcrops on the volcano itself and the immediate beach area exhibit sufficient correlation to permit accurate phase estimation. Thus, deriving topography using repeat pass interferometry at C-band in the Aleutian Islands in winter (data were collected in December) is at best a risky proposition.

Digital elevation models and baseline estimation from tie points. Once we have determined image pairs exhibiting sufficient correlation over large ground areas, we can proceed to form the interferograms and reduce them to height models. We determine the relative phases of all the points in the interferogram using the phase unwrapping algorithm of Goldstein *et al.* [3], which adds the proper multiple of 2π to each phase measurement.

Equations (1-3) gives the relation between the path difference for a given baseline and the phase measured in the interferogram, assuming parallel orbits. In actuality, the ERS-1 orbits converge slightly, not enough to alter the along-track pixel spacing, but enough to induce an along-track component to the measured differential phase. In terms of (1), this situation can be approximated by

$$\delta = \frac{\lambda}{4\pi}[\phi - m_x x + \phi_0] \tag{12}$$

where x is the along-track position, m_x is the orbit convergence phase rate, and ϕ_0 is a constant phase. We already noted that. tiepoints are necessary to determine the absolute height on the surface. We have implemented this as an empirical baseline estimation scheme, where the baseline magnitude B, orientation α, and along-track phase parameters are determined from equations (12), (2), and (3), using the unwrapped image phases at the tiepoints in (12) and ma~)-derived height measurements in (3). This was done for the images here by fixing the vertical component of the baseline B_z to 10 meters times the orbit repeat time (the ERS-1 orbit decays by 10 m per day) and computing the cross-track baseline component B_y, m_x and ϕ_0 from three tiepoints in the scene.

This completely empirical approach is both expeditious, as it is extremely difficult to obtain high accuracy orbit reconstructions, and it is necessary, because the orbit reconstructions do not provide the absolute height accuracy we require. An alternate approach is also possible, in which accurate orbit information is used as much as possible, and then tiepoints applied to correct for a

height offset. However, the resulting accuracies will be similar, and still dependent on the tiepoints.

Once the baseline and along-track phase parameters are determined, equations (12), (2), and (3) provide a conversion from the unwrapped phases to height: the three-dimensional coordinates of each pixel are known and the pixel can be placed on a ground coordinate grid. We choose an assumed spherical earth with radius equal to the geodetic radius at the center of the image for our reference surface here. When the points are placed on the grid, a map such as the one shown in figure 7 results. Figure 7 is a reduction of data collected over the Toolik site and is the same 3 day orbit pair shown in figure 3b. Here radar brightness is shown as the brightness of each point, and the color is determined by the altitude, While in digital format we retain the actual height value, for the display we quantize the heights as described in the figure caption.

Note that a number of 'holes' remain in the figure. Although the original radar image is continuous in the radar slant range and azimuth coordinate system, mapping onto a ground coordinate reference surface illustrates that there are places for which height estimates are not available. Three principal causes for the undetermined phases exist. First of all, due to foreshortening or 'layover' effects, in areas where the surface slope approaches the incidence angle, the ground range resolution becomes much larger than the output range pixel spacing, so that a single measurement characterizes many output pixels. Since we map each measurement only at the point corresponding to the center of the resolution cell, several points in the output grid remain unfilled. This effect dominates al low incidence angles such as the 24° used by ERS-1.

The second effect is that of shadowing. Similar to optical shadows, radar shadows are formed when a taller object intercepts the illumination which would have illuminated a shorter object behind the first. Since no echo is available in these regions, no phase estimate is available. This effect becomes most important as grazing incidence geometries are used, and is negligible for ERS-1.

Finally, there are regions for which the radar backscatter is simply too low or the signals are not at all correlated over time so that accurate phase estimation is impossible. In these cases the phase unwrapping algorithm identifies the region and no attempt is made to obtain height estimates.

We have chosen to overcome the 'hole' problem by linearly interpolating in ground range over the blank areas, assuming that the surface itself is smooth over the scales of interest. A sample map is shown in figure 8, a height map of the Toolik site with all corrections applied. Note that in wide blank areas such as to the left at the top or middle of the image, the simple linear interpolation scheme adapted introduces height artifacts. Some of these artifacts can be removed using a different interpolation scheme, however such schemes use data two-dimensionally and are generally quite computationally inefficient. Linear interpolation serves to demonstrate the ERS-1 height mapping capability. Figure 9 is a perspective view of these data where altitude and radar backscatter are converted into hue, saturation and intensity to make a pleasing and natural effect.

We present in Figure 10 a perspective view generated from 35-day repeatpass ERS-1 data of the

Pisgah lava flow in California. This image was corrected for absolute heights with tie points and exhibits statistical uncertainties of about 3 m rms in the flat areas. This desert region undergoes little weathering in the summer (data were acquired in August and September), demonstrating that under the proper conditions the repeat-pass implementation can be used with long repeat cycle radar systems. These long cycles are required for global coverage, thus data may in principle be obtained worldwide and reduced topographically. However, environmental factors probably limit the usefulness of the data set to selected regional studies.

Accuracy of the Alaska ERS-1 DEMs.

Accurate digital elevation models of Alaska do not exist and this greatly constrains our ability test the accuracy of our approach to topographic mapping. We can, however, analyze the performance of the mapping procedure in a number of ways: 1) we can spot check the altitude of obvious features with conventional topographic maps, 2) we can compute the statistical errors over flat areas to ascertain whether or not they agree with theory, and 3) we can evaluate statistically the expected height standard deviation from a baseline derived from a typical tiep oint set.

Table 4 gives the results of applying procedure 1, examining the elevation of specific features in the Toolik site data:

Table 4. Elevation Spot Checks of Toolik Site Features

Feature	Elevation USGS Map	Elevation ERS-1 Radar	Delta
1. Small lake near Sag River	611	613	1
2. Toolik Lake	719	718	1
3. 2nd lake near Sag River	507	505	2
4. Imnavait Mountain	1122	1102	20
5. Slope Mountain	1223	1221	2
6. Small hill near Toolik Lake	930	942	12

We note that the maps agree within two meters in the first three areas chosen but diverge slightly on estimates of the mountain peaks chosen for the latter three sites. In fact the very close agreement seen on the flat regions is due more to our implementation which used estimates in those areas as tic points to determine our baseline distance and the degree of convergence of the orbits. The realized precision of the technique is better demonstrated by the remaining values which range from 2 to 20 meters. Since accurate digital elevation models of these areas are not available for truthing investigations we are limited by the ability to identify features on 200 foot contour maps. It is very difficult to identify the peaks of the mountains which typically do not have measured benchmarks, and we must interpolate the contours to obtain height estimates from the USGS maps. Even with USGS map benchmarks, precisely locating the corresponding point in the interferogram

is very difficult.

We call, however, measure the statistical variation in flat areas and compare the results to the nominal prediction. For example, if we choose the flat region near Toolik Lake in the 3 day image, we obtain an rms height deviation of 2.5 m. We noted previously that a correlation of 0.25 corresponds to 7.5 m height error. The 2.5 m error (3 times smaller) determined here is consistent with the correlation of 0.75 (3 times larger) in this region seen in fig. 3b.

In figure 11 we present the digital elevation model derived from data acquired over the! Manley Hot Springs site. Here the rms height error over the flat region in the center of the image below the river is about 2.0 m, less even than that found in the Toolik data set, as the temporal correlation here is 0.85. The elevation spot check results are shown in Table 5. Again the flat areas are quite close and the two mountain peaks chosen exhibit 3 and 31 meter errors.

Table 5. Elevation Spot Checks of Manley Hot Springs Site Features

Feat urc	Elevation USGS Map	Elevation ERS-1 Radar	Delta
1. Lakes south of Hot Springs	84	83	1
2. River near Cosna	76	71	5
3. Small lake north of Bear Lake	197	193	4
4. Small hill near Bear Lake	269	266	3
5. Mooseheart Mountain	651	620	31

For procedure 3, we have developed a statistical method to evaluate the errors in the baseline and the consequent RMS height error over an image, as follows. Fiducial heights were read from a USGS topomap (National Geodetic Vertical Datum of 1929). Each height tiepoint was located in the 3-day repeat Toolik interferogram, such that a database of tiepoints was generated, including row, column, height, phase and phase variance. The relative ranges of spacecraft to any point (row, column) in the image are well known, so the database information is sufficient to reconstruct the interferometric baseline.

For N tiepoints, we randomly chose M sets of K tiepoints, where K < N. The random draw was done so that no set of K tiepoints contains a duplicate tiepoint, no two tiepoint sets are the same, and the tiepoints in a set span a sufficient image area to give a good baseline estimate. For each of the M sets, a baseline was computed according to the methods outlined previously. In this way we generated a set of baseline estimates from which we can develop an intuitive and statistical sense for the robustness of the technique. in particular, for each baseline estimated, the height at each image tiepoint can be reconstructed. The residual between the reconstructed height and the height measured from the map can then be used as a measure of tile success of the technique.

The residual for only the tiepoints used to form the baseline estimate is usually small, on the order of 5 to 10 meters. However, the residual over all image tiepoints is never less than about 15 meters, and is frequently much greater. This is consistent with the spot check method in which the height errors near the tiepoints used 10 form the baseline were small.

To evaluate the effects of noise more carefully, we simulated the interferometric phase by solving the forward problem: given a height, nominal baseline and azimuth ramp, what is the interferometric phase? We then added Gaussian noise to the simulated phase and to the heights to model the effect of data noise and topographic map measurement noise.

In the presence of noise, it is virtually impossible to estimate the physical baseline (two cross track components) while also estimating a linear phase ramp in azimuth (slope and intercept) with only a few tiepoints. The variation of the interferometric phase with baseline orientation is sinusoidal and is essentially the same for all look angles. This orientation-dependent phase constant can be absorbed in the phase constant for the azimuth ramp. Thus there is a large number of possible parameter combinations that can fit the data.

The solution is relatively insensitive to the assumed geoid as long as a local quadratic approximation to Earth curvature is accounted for. An incorrect assumed radius of curvature introduces errors of less than 1 meter. An incorrect geocentric (reference) radius introduces virtually no height errors, as it translates to a phase constant across the image, which is fitted and removed. 'Thus, by estimating an arbitrary phase constant, absolute height information is lost.

We performed three different tests on data simulated to have 5 meter random height deviations but no statistical phase errors. In the first test, four parameters were fit using 4 or more height tiepoints. For baselines from the best sets of tiepoints, those widely separated in range and azimuth, the residual height errors were on the order of a meter or less, corresponding to baseline estimates well matched to the simulated values. Over all the possible tiepoint sets, however, the estimated baselines differed significantly, and the average height residual deviation was never better than the 5 meter measurement errors. This reflects the correlation among fitted parameters. increasing the number of tiepoints decreases the height errors on average, .such that they approach the height measurement errors.

In the second test, three parameters were fit, with the fourth, the vertical component of the baseline, fixed at its simulated value. As expected, the horizontal baselines generally come closer to the simulated values, and the average height residuals approach 2 or 3 meters when using 7 tiepoints. The best baseline estimates again yield residuals of order 1 meter. It is impossible to know a priori if the tiepoints will yield a height residual better than the measurement error. Therefore, it is important to use as many tiepoints as possible in these estimates.

In the third test, we fixed the vertical baseline component to an incorrect value and fitted the remaining three parameters. It is now impossible to approach the exact baseline, and as a result,

the minimum height residual deviations increase to greater than or equal to the height measurement error, and the average height residual deviations also increase.

Thus in fitting 3 parameters, it is important to have a reliable estimate of the fixed parameter or to have small phase noise and height measurement errors. In fitting 4 parameters, it is important to use as many tiepoints as possible, and reduce the variance of the tiepoints' height error and tile data phase noise to levels of the desired height accuracy.

These results relate to the height maps in this work in the following way. These maps were generated by fixing the vertical component of the baseline and fitting the remaining three parameters, Three tiepoints were used for the fit. From our simulation (5 m height errors, no phase errors), the average height residual for this case was about 15 meters; the minimum residual was about 1 meter. For the 3-day repeat Toolik data, the average height residual was about 50 meters, while the minimum was about 15 meters. There is an essential difference between tile simulation residual calculation and the actual. The simulation residual is the difference of the derived heights and the heights with no noise. The actual residual by necessity must use the heights measured from the USGS map with the associated measurement noise. Therefore, the minimum residual variance is likely to be tile effective height variance of the data, that is a combination of the phase variance interpreted as height variance and the actual map height measurement variance. In this case, it is 15 meters. The upper limit on height error based on measured decorrelation and looks is about 7.5 meters. The small residual determined here using laborious hand measurements off a topomap is actually quite encouraging.

At the time of this work, an accurate orbit reconstruction was not available, so one of the baseline components was fixed, the other estimated. When an orbit reconstruction is available to 30 cm accuracy, we can fix both baseline components to their approximate values, and fit two parameters - just the along-track ramp. This case is similar statistically to rows 5-9 in Table 6, where three parameters were estimated, and B_z was fixed at its correct value. We can see that about 6 tiepoints of 5 m rms accuracy are needed to obtain an rms DEM height accuracy of 5 m. If the tiepoints heights can be measured in situ, for example with GPS receivers, rather than off a map, then the limiting tiepoint error is the phase noise. Five meter equivalent rms phase noise is achievable with ERS-1 data when decorrelation is small.

Table 6. Baseline Determination Simulation Results

Parameters γ_i	Tie Points Used	Mean σ_z Baseline Tie points	Mean σ_z All Tie points	Minimum σ_z, All Tie points	Maximum σ_z, All Tie points	B_z
4	4	3.87	27.41	1.72	116.23	
4	5	3.53	8.75	.39	28.62	
4	6	3.08	5.28	0.77	≥08	
4	7	2.58	6.10	0.49	29.78	
3	3	3.70	15.06	.27	33.02	30
3	4	2.74	7.71	0.13	53.53	30
3	5	2.69	5.07	1.21	18.49	30
3	6	2.24	3.43	o.76	10.92	30
3	7	1.93	2.45	0.08	5.10	30
3	3	3.70	29.95	7.06	127.81	−30
3	4	4.48	14.86	6.21	51.72	−30
3	5	4.83	12.62	6.28	30.77	−30
3	6	5.52	0.36	6.23	24.19	−30
3	7	4.81	8.80	5.95	15.04	−30

Simulation inputs:

B_z = 30 m

B_y = −233.167 m

ϕ_0 = 26937.2 rad

m_x = 4.01746×10^{-3} rad/m

phase standard dev = 0 rad

height st. dev = 5 m

Globa Mapping Possibili ies

Finally, n this section we discuss he possibility of obtaining a global topographic map using he ERS- satellite and radar system. Global mapping of he Earth by repeat orbit procedures is feasible only if a suitable orbit and coverage scenario is used. As we have seen that temporal decorrelation phenomena can dominate the measured phase over many types of terrain, the orbit repeat time must be minimized to achieve high correlation on successive echoes. As the ERS-1 critical baseline is 1115 m, to keep baseline decorrelation to a feasible value the repeat geometry must be such that the satellite returns to the same point relative to the ground within 200 m; in addition the set of imaged swaths must cover he Ear h in a reasonably short time, a year or less

We propose the following implementation as optimal for a satellite identical to ERS-1. An orbital altitude of 561 km provides a one day repeat interval. Even at this relatively short repeat interval the possibility remains that environmental factors such as rain or snow could decorrelate the echoes over wide areas. At a reduced altitude of .561 km, the look angle may be increased to 40° while achieving the same noise equivalent radar signal to noise ratio of 11.7 dB, improving the current ERS-1 problem with layover. However, as the normalized cross section of most targets decreases with increasing angle some degradation of signal to noise ratio will occur. In this imaging geometry the usable swath, defined as the 1.5 dB points on the one-way antenna pattern, is 50 km.

The imaging scenario is as follows: First, map a single 50 km swath for one day, then, repeat this coverage to obtain interferometric data over the swath on the second day. A single day period comprises 15 imaging swaths for a total illuminated width of 750 km at the equator if only ascending or descending passes are considered. The data may then be processed and checked for gaps due to temporal phenomena and if desired the missing areas may be reacquire'd. At this point the orbit node must be advanced about 40 km for the next pair to allow some overlap between swaths, and for a total equatorial distance of 40000 km 64 such maneuvers will be required. This would result in complete equatorial coverage.

Since the orbits converge at t he poles, the interferometer baseline will at some point become too short and the errors will become unusably high. If we select 75 m as this minimum baseline, corresponding roughly to a factor of three decrease in single-image accuracy, the maximum useful orbit latitude is 68°. However, multiple coverage at the higher latitudes permits some averaging so that the total accuracy decrease is less than tile factor of three expected from the baseline variation alone. This misses the polar regions but does obtain topographic data over most of the Earth's land surface.

We must note here that the above assumes that we have several tie points distributed in range within each segment of the radar swath- the size of the segment is determined by the orbit stability. These tie points will in all likelihood not be distributed evenly across the Earth's surface, thus the accuracy of the maps produced will vary widely with the quality and number of tic points. Since the precision of maps obtained with ERS-1 can exhibit values as poor as 12-15 m for unfavorable orbit latitudes and locations with large temporal decorrelation, such a piecemeal global data set is not significantly superior to what is available now. However, for regional studies of selected sites for which either absolute accuracy is unimportant, or for which tie points are readily obtained, the ERS-1 derived digital elevation models will be invaluable.

We note that if precision orbit determination is possible on a future satellite, such as the 3 cm suggested by experiments involving the Global Positioning Satellite on the NASA TOPEX ocean altimeter mission, the absolute accuracy problem becomes less of a constraint. Assuming a 200 m interferometer baseline, an orbit height uncertainty of 3 cm for each orbit and equations (6) give a resulting absolute height error of SO III for a 561 km orbit at a 40 degree look angle. Thus, orbit

determination alone can achieve somewhat accurate absolute heights, but tic points will be required to reduce the absolute error to the 2 m levels obtained from statistical signal variations.

In order to reduce the absolute height errors, the spacecraft could be equipped with a nadir-looking laser altimeter to obtain tie points with which to minimize absolute height and slope errors. The laser would also obtain many good measurements over the polar regions which 1) are not mapped well by a repeat pass radar due to the converging orbits and hence small baselines and 2) are relatively flat and do not need the radar system's ability for high spatial resolution. Since the radar resolves the local topography, the laser tie points may be quite sparse every 10 km or so would suffice. The locations of the reference points must be very accurately coregistered with the radar data, a nontrivial task in itself, Of course the reference points will be available as weather permits; the laser system will not work over cloudy regions at all. 'J'bus, the success of this implementation in terms of reducing the absolute error levels to those associated with relative measurements depends on the ability to generate a high-quality auxiliary data set.

summary

Topographic maps with relative errors of 5 m rms or less can be derived from interferometric radar data collected by the ERS-1 radar system, providing a relatively inexpensive means to generate digital elevation models over regions of the Earth where little or no topographic data is available. This method would also yield a consistent approach to obtaining high resolution topography over different areas; a consistent worldwide data set dom not exist today. We have derived digital elevation models from ERS-1 data acquired over Toolik Lake and Manley Hot Springs in Alaska and over part of the Mojave desert in California. Since 1) temporal decorrelation at the C-band wavelength can yield DEMs with poor height acuity, and 2) orbit uncertainties necessitate the use of tie points to minimize absolute height errors, regional studies can be accommodated but global mapping with the satellite would not result in a data set significantly superior to what is already available. While these effects can be mitigated by utilizing a satellite orbit with a shorter revisit time and more precise orbit determination, such as that provided by GI 'S, it is unlikely that the uncertainties of the measured heights could be reduced to levels acceptable for precise global topographic applications. The existing, and proposed improved, ERS-1 systems do promise, however, the ability to generate a new set of topographic data that will prove useful for many discipline studies.

Acknowledgements.

The research described in this paper was carried out by the Jet Propulsion Laboratory, California Institute of Technology, under a contract with the National Aeronautics and Space Administration.

Figure captions.

Figure 1. Interferometer imaging geometry. Two antennas Al aud A2 both illuminate the same patch of ground. Surface topography is given by $z(y)$, the spacecraft altitude is h shove a tangent

plane at the point of interest, the baseline distance is B, the range to a point on the ground is r, the look angle is θ, and the angle of the baseline with respect to horizontal is α. The radar signals transmitted from each antenna and received at the point of transmission will form an interferogram where the phase at each point is proportional to the difference in path lengths, δ, with the constant of proportionality $\frac{4\pi}{\lambda}$.

Figure 2. Uncertainty in interferometer phase as a function of correlation and number of looks.

Figure 3. Correlation maps of the Toolik Lake site, derived from orbit pairs 943-1029 (6 day interval, 3a) and 1029-1072 (3 day interval, 3b). Zero correlation is represented by bluish purple, while unity correlation is given by yellowish green. The majority of the six day image possesses an average correlation of 0.50 or more. The three day image has large areas in which the correlation drops below half. Since signal to noise ratios are similar and baseline decorrelation in both cases is small, the temporal correlation is higher over the longer rather than the shorter time interval. Environmental factors which occur sporadically rather than continuously over time are dominating the observed correlation.

Figure 4. Correlation map measured over the Manley Hot Springs site.

Figure 5. Correlation images of the Mt. Katmai area, showing that large sections of the region produce uncorrelated echoes. While certain subsections exhibit very high correlation values of about 0.85, only these small pieces may be expected to yield accurate phase estimates and hence useful digital elevation models. Figure 5a shows some evidence of an elevation effect, particularly on Mt. Griggs, the large mountain near the image center. The average of the correlation coefficients is greater than 0.,5011 the lower slopes of the mountain, but above a constant altitude it drops to the 0.28 average magnitude value expected for lo-look uncorrelated signals. The correlation in figure 5b is less obviously related to altitude but appears to be highest in the valley floors.

Figure 6. Correlation map of Shishaldin volcano in the Aleutian Islands. The ocean is completely uncorrelated, as is the laud area over much of the image. Only a few outcrops on the volcano itself and the beach area exhibit sufficient correlation to permit accurate phase estimation.

Figure 7. Height map of the Toolik site from the same 3 day orbit pair shown in figure 3b, geocoded but uot interpolated. There are a number of large and a plethora of smaller 'holes' in the image due mainly to foreshortening effects (see text). Here radar brightness is shown as the brightness of each point, and the color is determined by the altitude. While in digital format we retain the actual height value, for the display we quantize the heights to multiples of 18.75 meters and map each to a 16 element repeating color wheel. Thus the color repeat interval, say from red to red, for this map is 300 meters.

Figure 8. Data from figure 7 after linear interpolation. Color repeat interval is 300 meters.

Figure 9. Toolik, Alaska data from figure 8 in perspective view. The colors and intensities in this and the following figures were chosen for aesthetic appeal; blue does not represent water, green

vegetation, nor white Silo\V.

Figure lo. Perspective view of Pisgah lava flow generated from 35-day repeat cycle data. See caption to figure 9.

Figure 11. Perspective height map of Manley Hot Springs site. See caption to figure 9.

REFERENCES

[1] Zebker, H. and R. Goldstein, Topographic Mapping from Interferometric SAR Observations, Journal of Geophysical Research v.91, No. B5, p. 4993-4999, 1986.

[2] Zebker, 11 A., S.N. Madsen, J. Martin, K.B. Wheeler, 'J'. Miller, Y. Lou, G. Alberti, S. Vetrella, and A. Cucci, The TOPSAR Interferometric Radar Topographic Mapping Instrument, IEEE Transactions on Geoscience and Remote Sensing, to appear September 1992.

[3] Goldstein, R. hi., H. A. Zebker and C. Werner. Satellite radar interferometry: two-dimensional phase unwrapping, Radioscience, vol. 23, 110. 4, pp 713-720, July - August 1988.

[4] Gabriel, A.K., R. M. Goldstein, and H.A. Zebker, Mapping small elevation changes over large areas: differential radar interferometry, J. Geophys. Res. 94, No. B7, 9183-91, July 10, 1989.

[5] Gabriel, A. K. and R. M. Goldstein, Crossed orbit interferometry: theory and experimental results from SIR-B, Int'l Journal Remote Sensing, vol 9., no. 8, pp. 857-872, 1988.

[6] Zebker, 11 A., and J. Villasenor, Decorrelation in interferometric radar echoes, IEEE Transactions on Geoscience and Remote Sensing, vol. xxx, **110.** xxx, 1992.

[7] Prati, C., F. Rocca, and A. Monti-Guarnieri, SAR interferometry experiments with ERS-1, submitted to IEEE Transactions on Geoscience and Remote Sensing, 1992.

[8] Rodriguez, E. and J. Martin, Theory and design of interferometric SARs, Proceedings of the IEE, vol. 139, 110. 2, 1992.

[9] Li, F. and R.M. Goldstein, Studies of multi-baseline spaceborne interferometric synthetic aperture radars, IEEE Trans. Geo. Rem. Sens., vol. 28, no. 1, pp. 88-97, January 1990.

[1 o] Rodriguez, E. R., Maximum likelihood estimation of the interferometric phase from distributed targets, in press, IEEE Trans. Geosci. Rem. Sens., 1991.

[11] Quality estimates in data files consisting of Precisé Orbit Determination Solutions, as described in "German PAF ERS1 RAT Product Specification: Precise Orbit," ERS-D-PSD-30000, May 31, 1990.

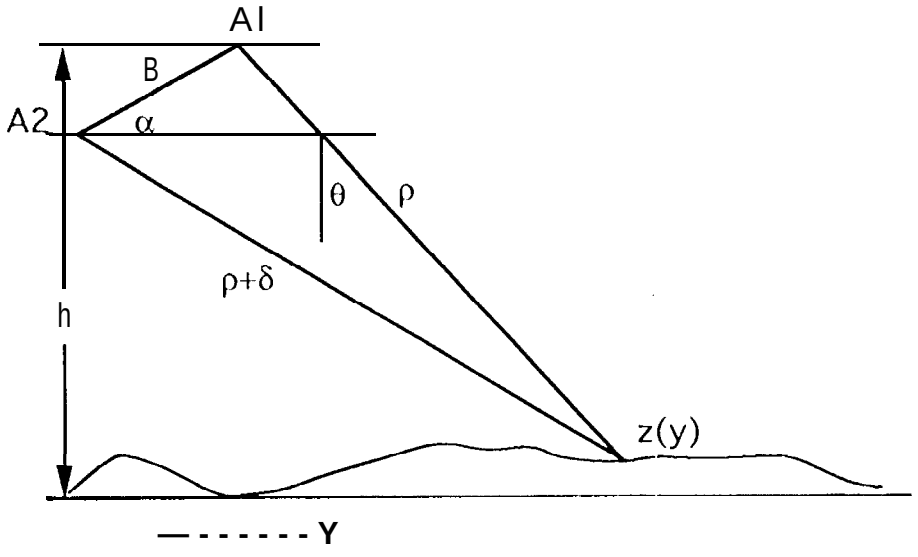

Figure 1 Zebker and Werner, 1992

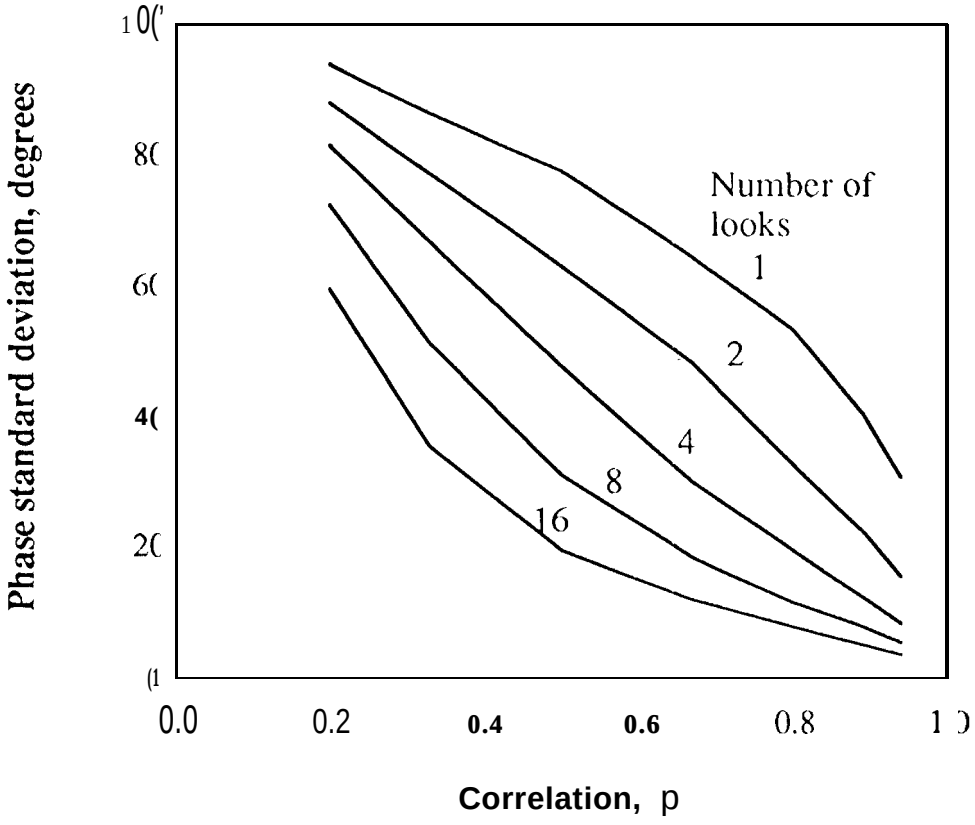

Figure 2. Zebker and Werner, 1992

TOOLIK LAKE

REVS 943. 1029 (6 DAYS)

REVS 1029. 1072 (3 DAYS)

0

1

CORRELATION

MANLEY HOT SPRINGS

REVS 892, 935 (3 DAYS)

0 1

CORRELATION

MT. KATMAI

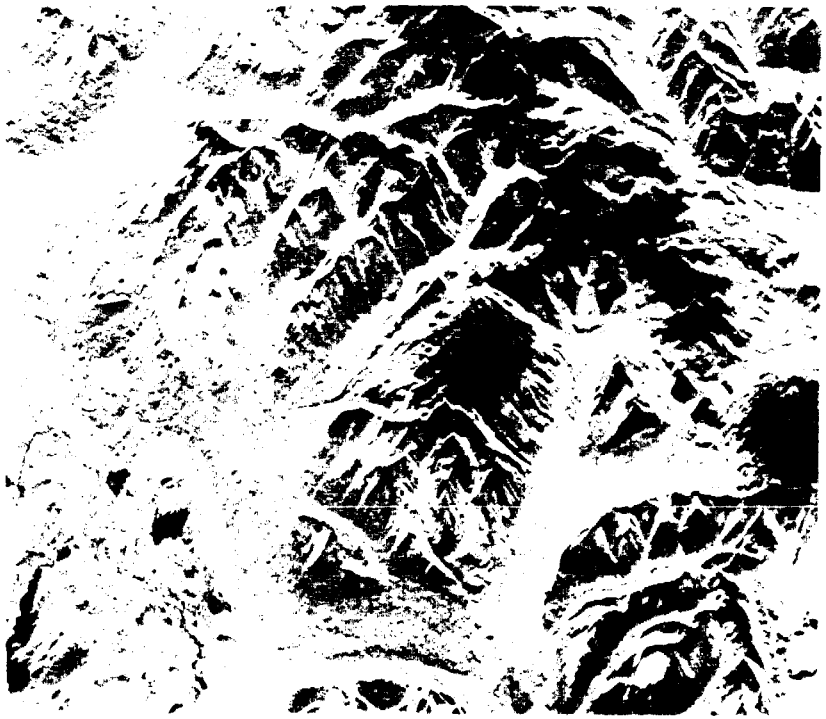

REVS 943.1029 (6 DAYS)

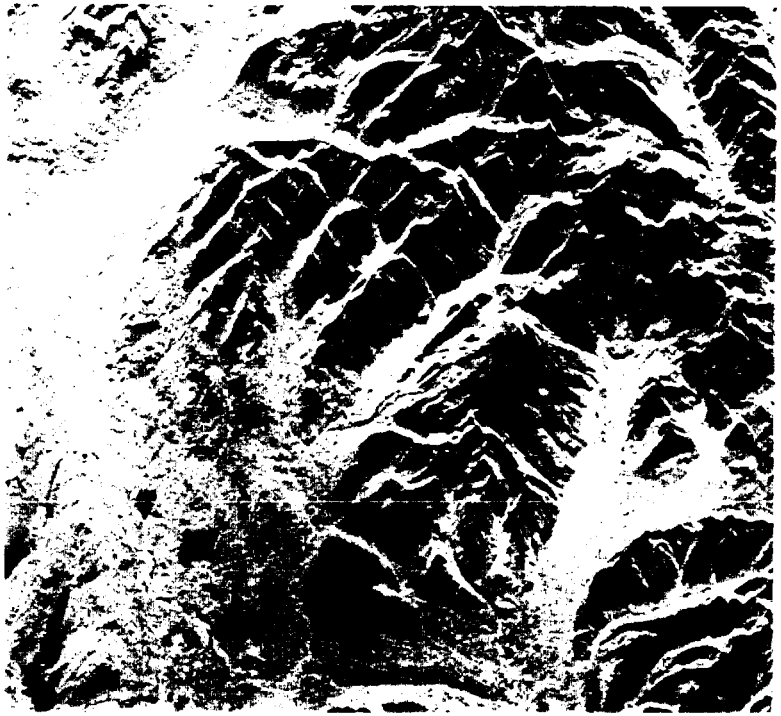

REVS 1459,1502 (3 DAYS)

0

1

CORRELATION

SHISHALDIN VOLCANO

REVS 2670, 2713 (3 DAYS)

0 1

CORRELATION

TOOLIK LAKE

ERS-1 DIGITAL ELEVATION MODEL

TOOLIK LAKE

ERS-1 DIGITAL ELEVATION MODEL

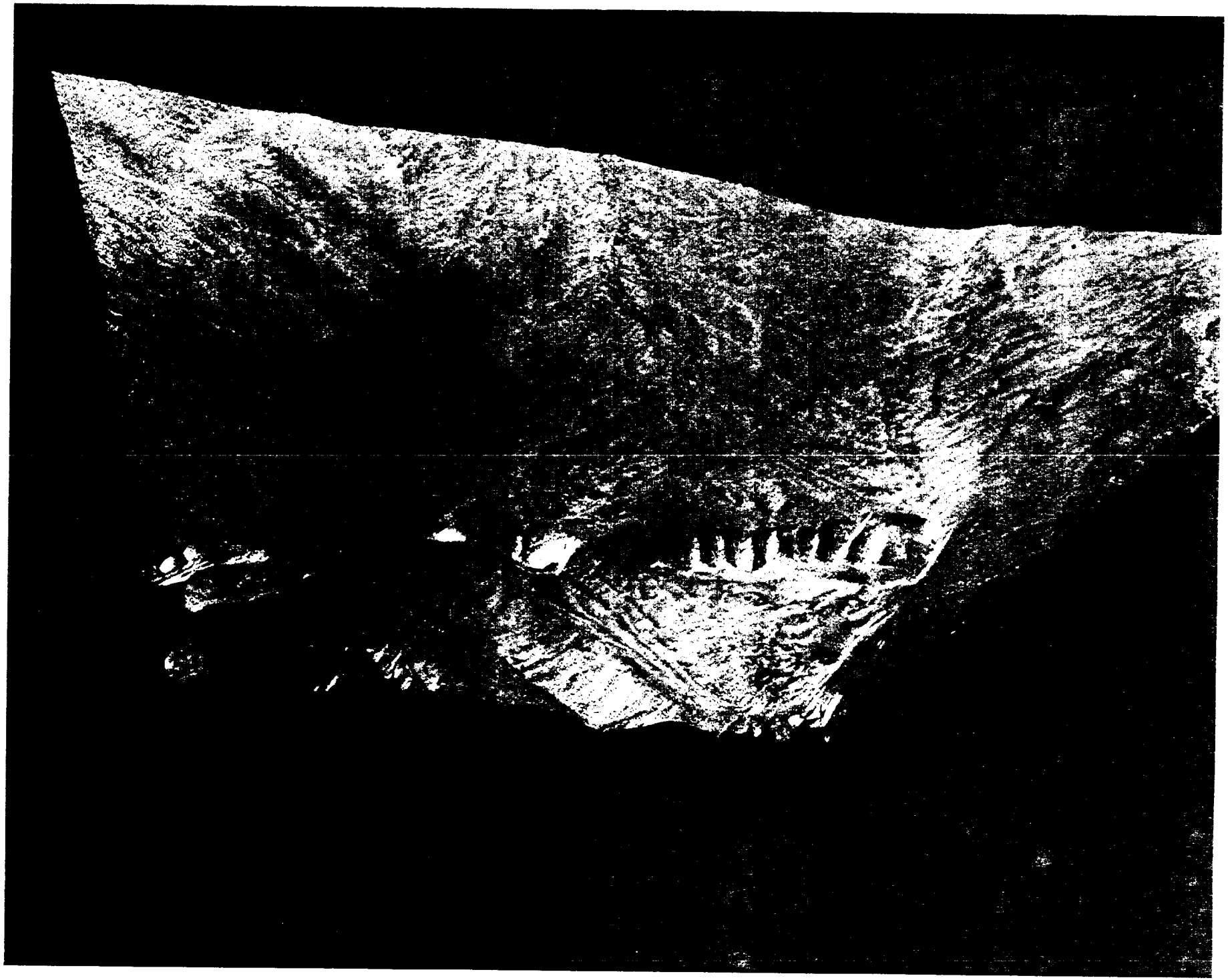

JPL

PISGAH LAVA FLOW, MOJAVE DESERT, CA
DIGITAL ELEVATION MODEL

ERS-1 INTERFEROMETRIC RADAR DATA AUG 23 / SEPT 27, 1992